Supplement of Atmos. Chem. Phys., 22, 15747–15765, 2022
https://doi.org/10.5194/acp-22-15747-2022-supplement

Atmospheric Chemistry and Physics
Open Access

Supplement of

Fundamental oxidation processes in the remote marine atmosphere investigated using the NO–NO_2–O_3 photostationary state

Simone T. Andersen et al.

Correspondence to: Simone T. Andersen (simone.andersen@york.ac.uk)

1 Calculations of Photolysis Rates

1.1 Photolysis Frequencies

The spectral radiometer located at a height of 7.5m provides a direct measurement of solar actinic UV flux and thus determination of atmospheric photolysis frequencies. The instrument consists of a 2-pi sr quartz diffuser coupled to an Ocean Optics spectrometer via a 10m fibre optic cable. It operates between 200 and 1000nm, calibrated between 250-750nm at 1 nm resolution. It utilises a Hamamatsu, back-thinned FFT-CCD detector with >90% quantum efficiency at 700nm. It has an integration time of 1 minute.

The instrument was calibrated in 2016 and again in 2019 against a 1000 Watt (FEL) quartz-halogen tungsten coiled coil filament lamp at the University of Leeds (Gooch and Housego NIST traceable FEL 1000-Watt lamp Standard of Spectral Irradiance (OL FEL-A)) bearing the designation F-1128. Providing the fibre optic cable isn't changed the calibration is relatively constant over a number of years (~7% drift in 10 years, (Bohn et al., 2016)).

47 photolysis rates are calculated using Python code developed by L.K. Whalley at the University of Leeds based on accurate absorption cross section and quantum yield from literature (http://chmlin9.leeds.ac.uk/MCMv3.3.1/parameters/photolysis.htt)

Solar radiation is measured from the same location with a Campbell Scientific sensor, SP-110 pyranometer. The sensor measures total sun and sky solar radiation over a spectral range 360 to 1120 nm encompassing most of the shortwave radiation reaching the surface. It measures a maximum of 1000 W m-2 (200mV) in full sun, 0.2mV per W m-2 at 5% accuracy.

1.2 jO(^{1}D) Calibration

Due to straylight issues affecting the spectrometer at the lower wavelengths (Bohn and Lohse, 2017) which can lead to errors in the calculation of photolysis frequencies such as $j(O^1D)$, following the subtraction of the dark signal, a linear fit is applied to the raw signal between 270 nm to ~285 nm where no ambient radiation is present and is extrapolated to determine the contribution of straylight in regions of the spectrum where ambient radiation is present. The straylight contribution is then subtracted. To verify this correction, for 1 month in 2020 $j(O^1D)$ was further evaluated using a co-located measurement made with a jO(^{1}D) 2pi filter radiometer (Metcon GmbH) (Bohn et al., 2016).

The $jO(^1D)$ filter radiometer output is proportional to the corresponding photolysis frequencies and the absolute calibration was determined during an intercomparison exercise when the instrument was run alongside a reference spectroradiometer (Bohn et al., 2016). The data from the two instruments is shown below in Figure S1.

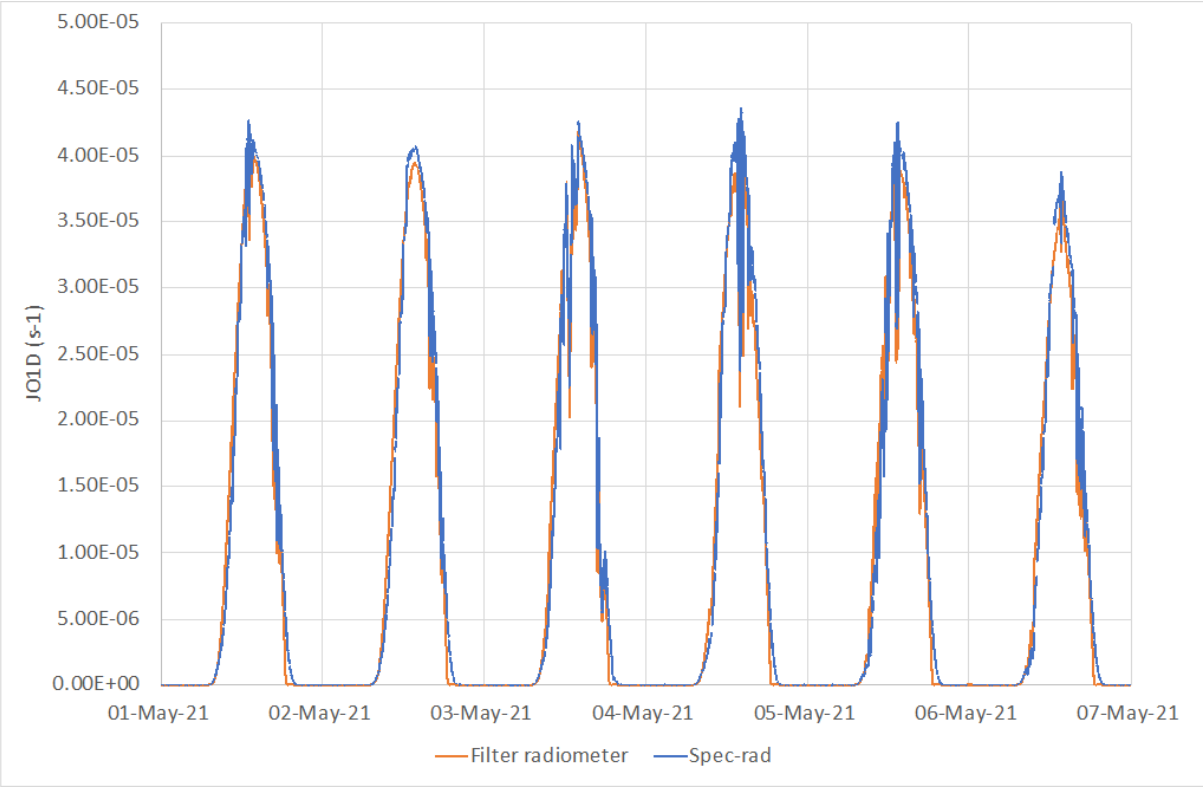

Figure S1: Comparison at the Cape Verde Atmospheric Observatory (CVAO) of $jO(^1D)$ measurements using a filter radiometer (NCAS, University of Leeds) and the core CVAO spectral radiometer.

1.3 Other Photolysis Rates

The calibration of the spectral radiometer in 2019 is assumed to be accurate for the calibration of other photolysis rates which photolyse further into the visible spectrum however the earlier calibration in 2016 may have been affected by reflections during the calibration procedure. As a result, the spectral radiometer observed more light through reflections than that directly emitted by the lamp, leading to a higher sensitivity than reality and under reading of the measurements in the early years. Therefore, we have used the correlation of photolysis rates with solar radiation in the 2020 between the hours of 9-5 pm to calculate the photolysis rates

prior to this date. An example of the correlation for jNO_2 can be observed in Figure S2 and the calculated photolysis rates are compared to the measured photolysis rates in Figure S3.

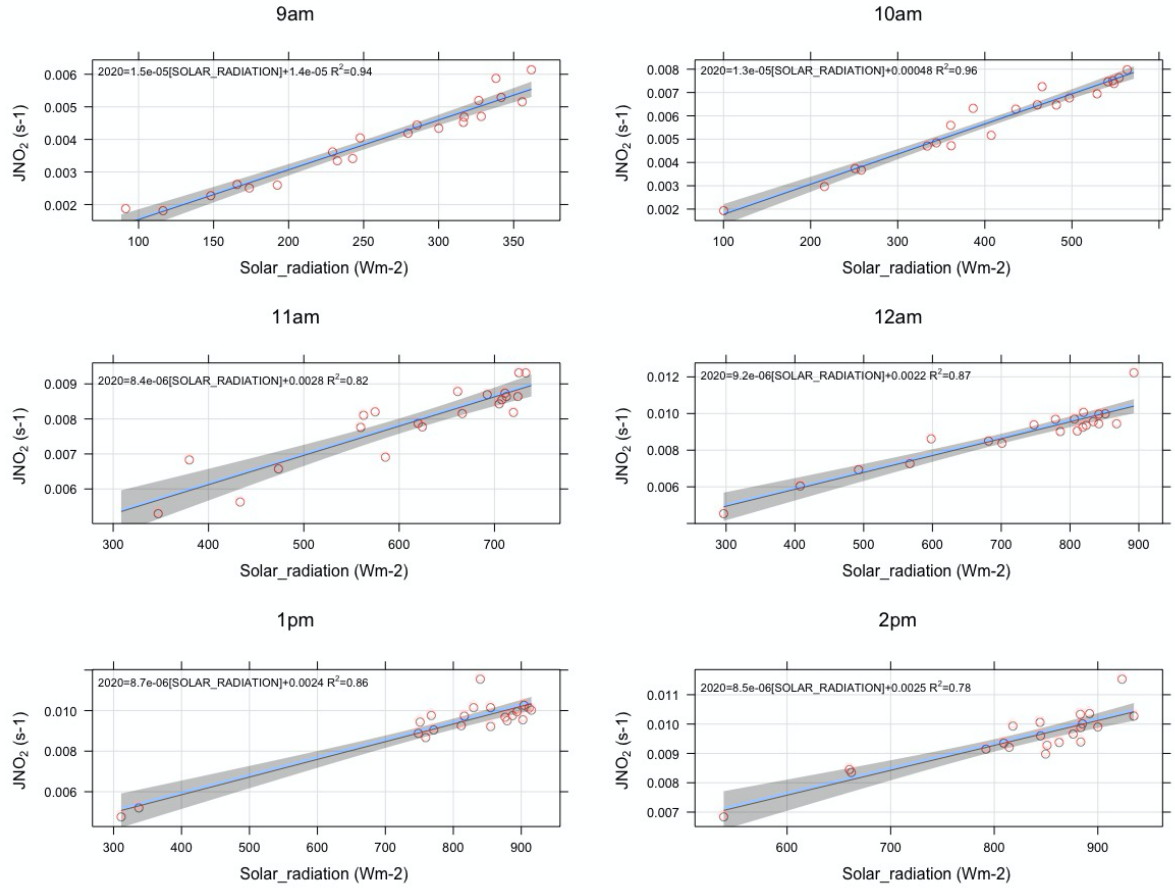

Figure S2: Correlation between measured jNO_2 from the spec-rad and total solar radiation.

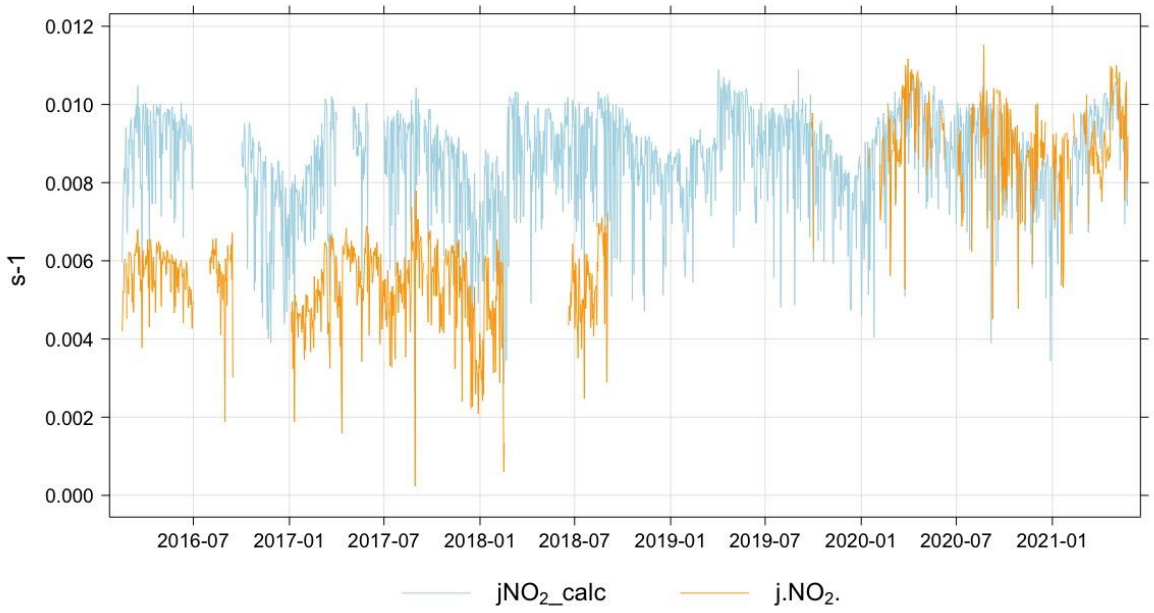

Figure S3: Comparison of measured *j*NO_2 and calculated *j*NO_2 for measurements at 2pm.

2 Figures

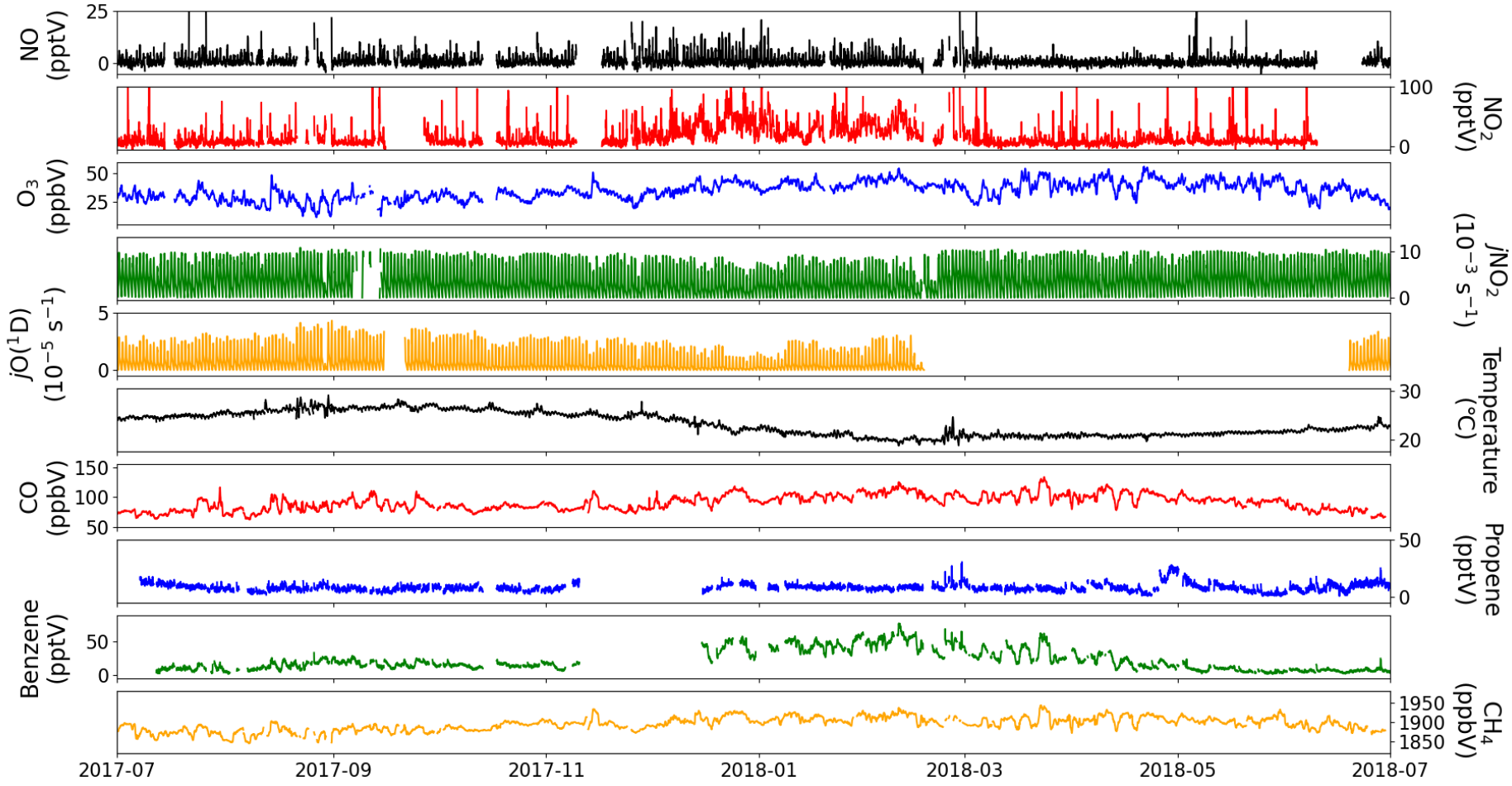

Figure S4: Time series of NO, NO_2, O_3, j_{NO2}, j_{O1D}, temperature, CO, propene, benzene, and CH_4 at the CVAO from July 2017 – June 2018.

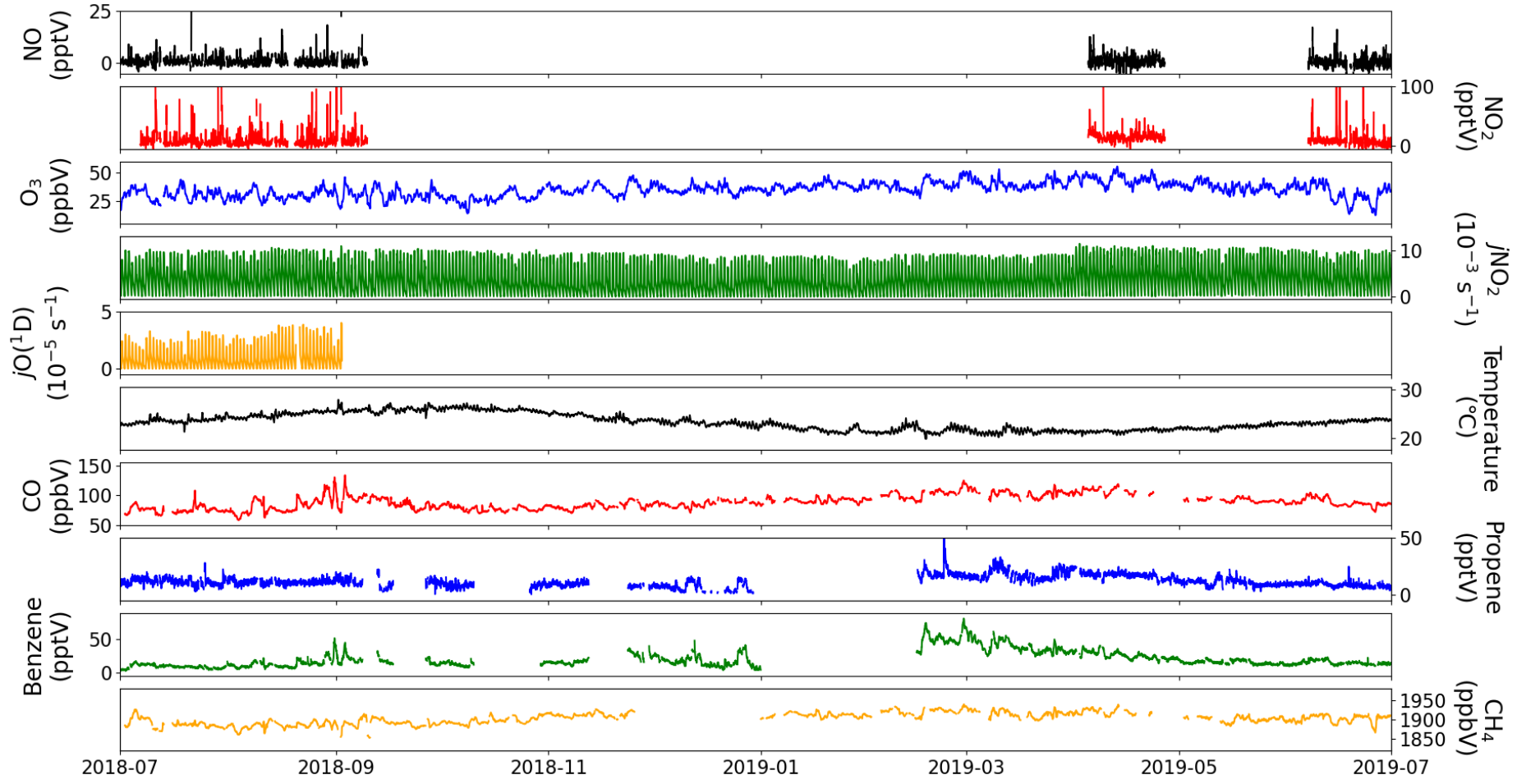

Figure S5: Time series of NO, NO_2, O_3, j_{NO2}, j_{O1D}, temperature, CO, propene, benzene, and CH_4 at the CVAO from July 2018 – June 2019

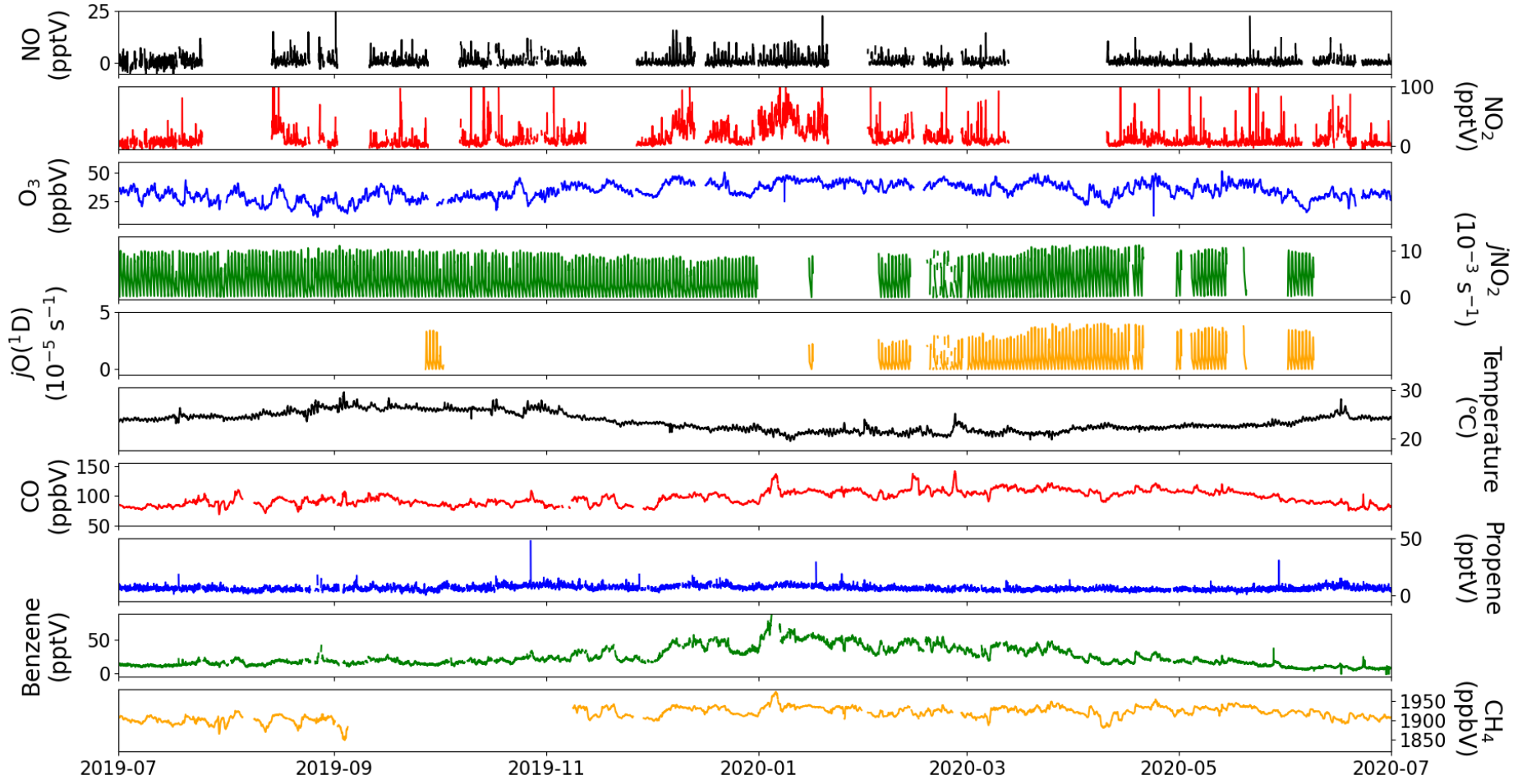

Figure S6: Time series of NO, NO_2, O_3, j_{NO2}, j_{O1D}, temperature, CO, propene, benzene, and CH_4 at the CVAO from July 2019 – June 2020.

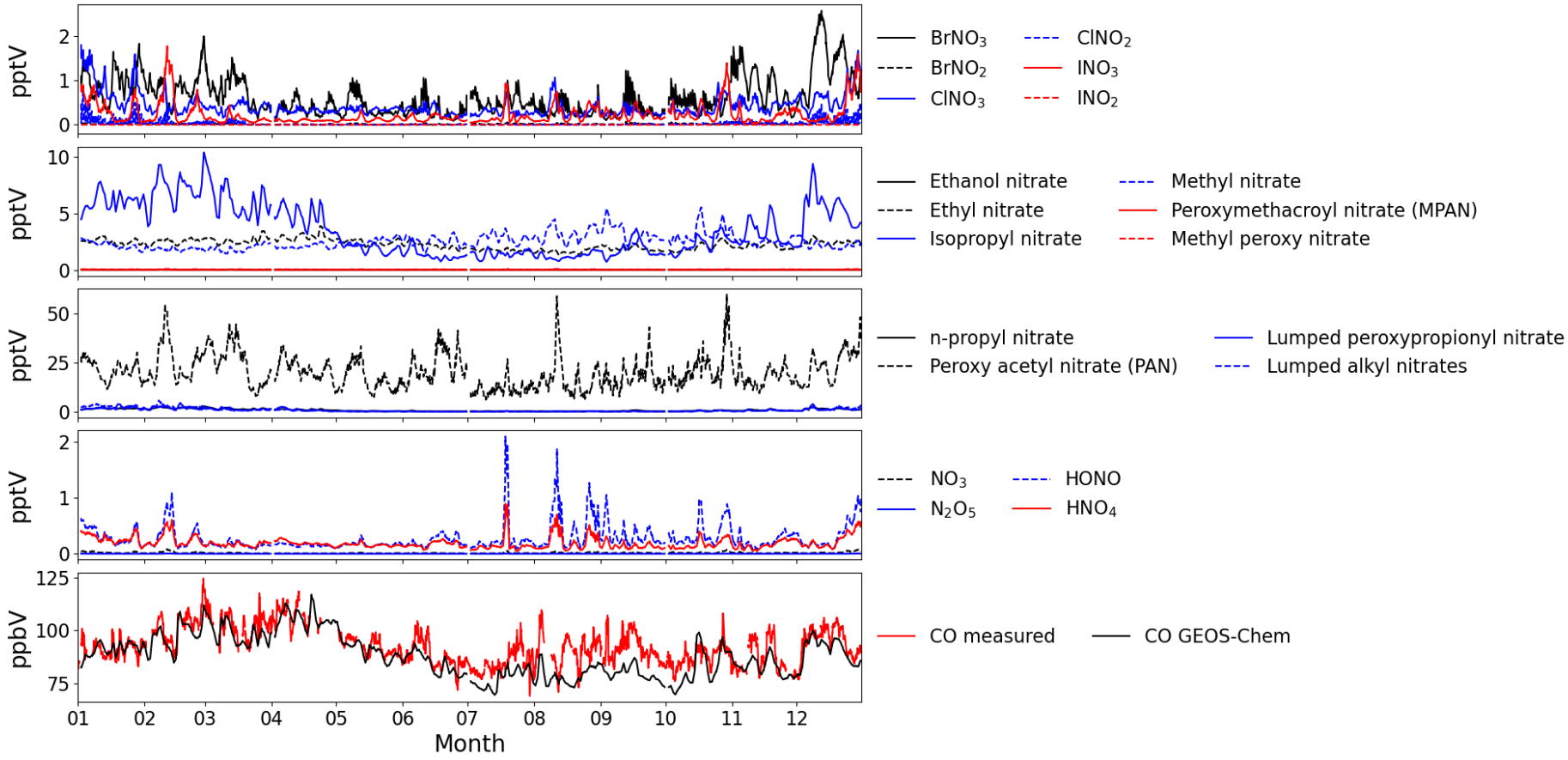

Figure S7: GEOS-Chem midday (11.00-15.00 UTC) model output for potential NO_2 interfering compounds and CO (pollution tracer) in 2019.

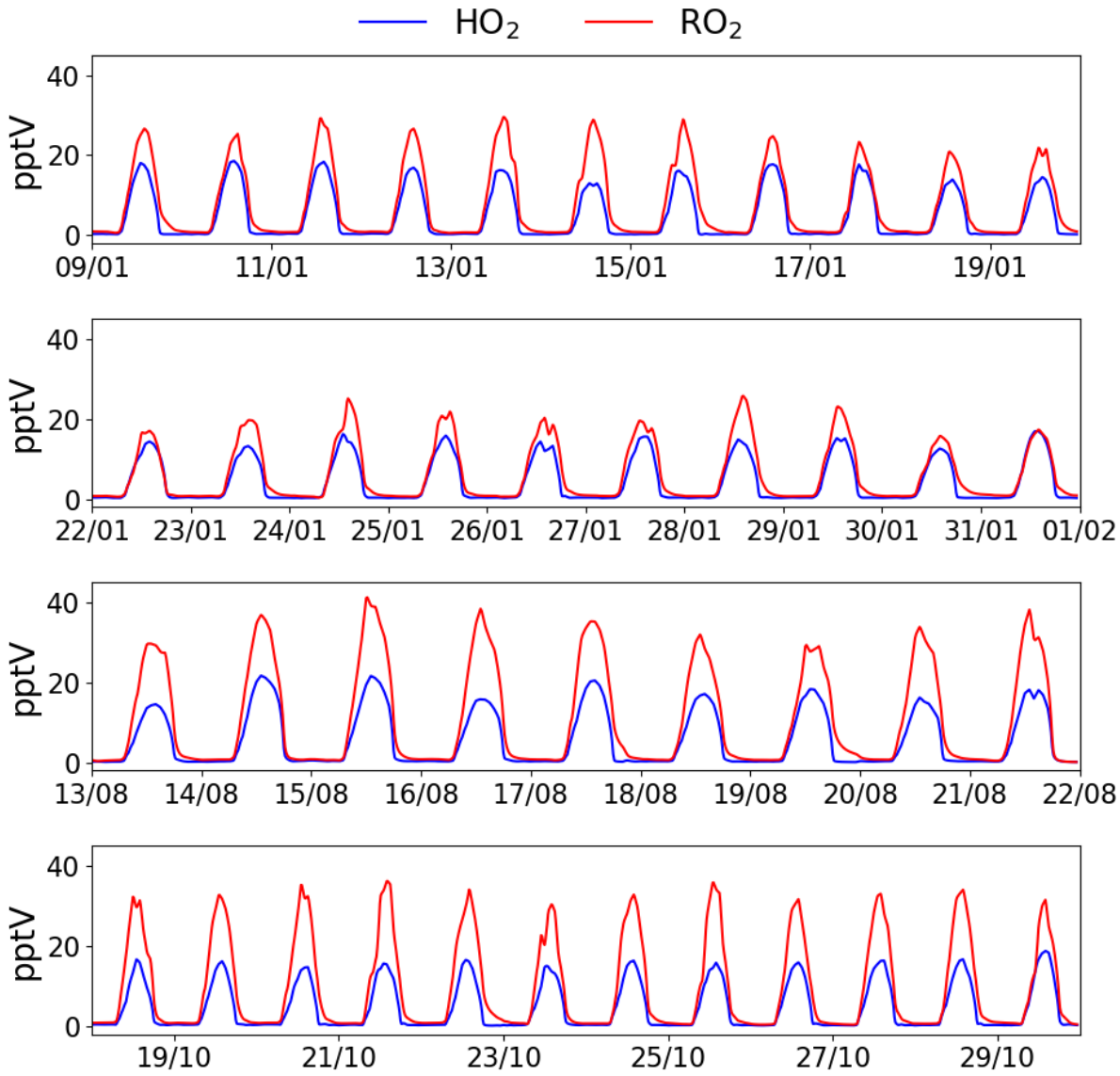

Figure S8: Daily modelled HO_2 (blue) and RO_2 (red) for January 2018, August 2017, and October 2017.

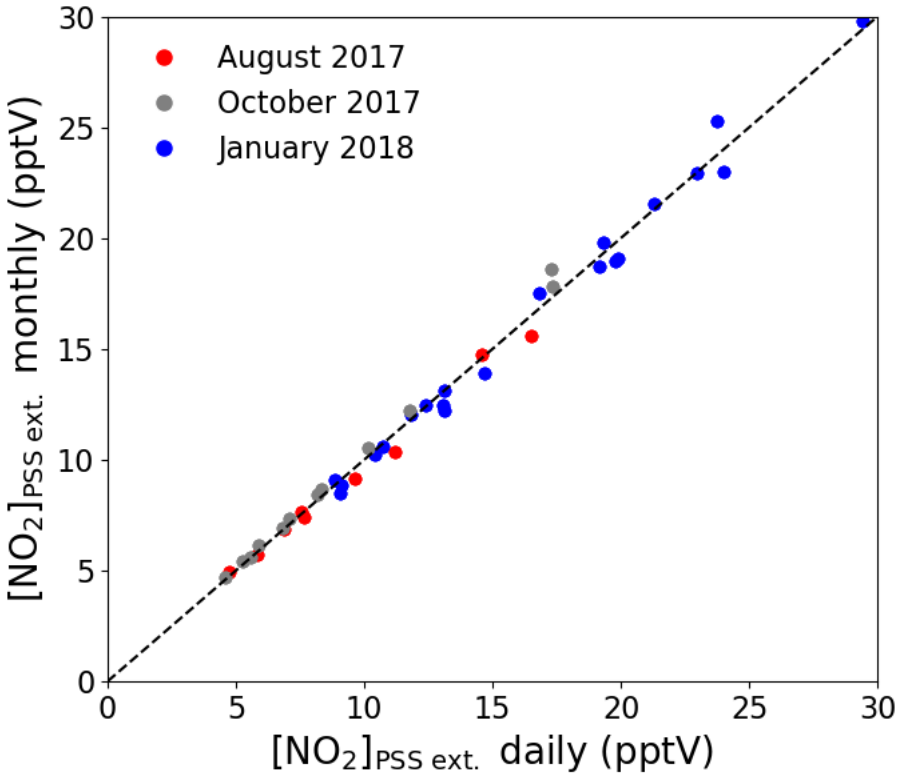

Figure S9: $[NO_2]_{PSS\ ext.}$ using monthly modelled diurnals for August 2017 (red), October 2017 (grey), and January 2018 (blue) have been plotted against $[NO_2]_{PSS\ ext.}$ using daily modelled diurnals. The dashed black line shows the 1:1 ratio.

3 Tables

Table S1: Reaction mechanisms added to the MCM

Bimolecular reactions	Rate coefficient (cm^{-3} $molecule^{-1}$ s^{-1})	Reference
$Br + O_3 \rightarrow BrO + O_2$	$1.6 \times 10^{-11} \times e^{(-780/T)}$	(Burkholder et al., 2019)
$BrO + HO_2 \rightarrow HOBr + O_2$	$4.5 \times 10^{-12} \times e^{(460/T)}$	(Burkholder et al., 2019)
$Br + HO_2 \rightarrow HBr + O_2$	$4.8 \times 10^{-12} \times e^{(-310/T)}$	(Burkholder et al., 2019)
$HBr + OH \rightarrow Br + H_2O$	$5.5 \times 10^{-12} \times e^{(200/T)}$	(Burkholder et al., 2019)
$BrO + NO \rightarrow Br + NO_2$	$8.8 \times 10^{-12} \times e^{(260/T)}$	(Burkholder et al., 2019)
$BrO + BrO \rightarrow 2\ Br + O_2$	$2.4 \times 10^{-12} \times e^{(40/T)}$	(Burkholder et al., 2019)
$BrO + BrO \rightarrow Br_2 + O_2$	$2.8 \times 10^{-14} \times e^{(860/T)}$	(Burkholder et al., 2019)
$Br + CH_3CHO \rightarrow HBr + CH_3CO$	$1.8 \times 10^{-11}\ e^{(-460/T)}$	(Atkinson et al., 2006)
$Br + HCHO \rightarrow HBr + HCO$	$7.7 \times 10^{-12}\ e^{(-580/T)}$	(Atkinson et al., 2006)
$I + HO_2 \rightarrow HI + O_2$	$1.5 \times 10^{-11}\ e^{(-1090/T)}$	(Burkholder et al., 2019)
$OH + HI \rightarrow I + H_2O$	3.0×10^{-11}	(Burkholder et al., 2019)
$IO + NO \rightarrow I + NO_2$	$8.6 \times 10^{-12} \times e^{(230/T)}$	(Burkholder et al., 2019)
$I + O_3 \rightarrow IO + O_2$	$2.0 \times 10^{-11} \times e^{(-830/T)}$	(Burkholder et al., 2019)
$IO + HO_2 \rightarrow HOI + O_2$	$1.4 \times 10^{-11} \times e^{(540/T)}$	(Atkinson et al., 2007)
$HOI + OH \rightarrow IO + H_2O$	5.0×10^{-12}	(Riffault et al., 2005)
$IO + IO \rightarrow I + OIO$	$5.4 \times 10^{-11} \times e^{(180/T)} \times 0.38$	(Atkinson et al., 2007)
$IO + IO \rightarrow I_2O_2$	$5.4 \times 10^{-11} \times e^{(180/T)} \times 0.62$	(Atkinson et al., 2007)
$IONO_2\ (+M) \rightarrow IO + NO_2\ (+M)$	$1.1 \times 10^{15} \times e^{(12060/T)}$	(Atkinson et al., 2007)
$OIO + OIO \rightarrow$ products	1.5×10^{-10}	(Gómez Martín et al., 2007)
$IO + OIO \rightarrow$ products	1.5×10^{-10}	(Gómez Martín et al., 2007)
$BrO + IO \rightarrow Br + 0.8\ OIO + 0.2\ I + O_2$	$1.5 \times 10^{-11} \times e^{(510/T)}$	(Atkinson et al., 2007)
Termolecular reactions	$n = (1 + (\log_{10}(k_0 \times [M]/k_\infty))^2)^{-1}$ $k = (k_0[M]/(1 + k_0[M]/k_\infty)) \times F_C^{\,n}$ $F_C = 0.6$ unless stated otherwise	
$OH + OH\ (+M) \rightarrow H_2O_2\ (+M)$	$k_0 = 6.9 \times 10^{-31} \times (T/298)^{-1}$ $k_\infty = 2.6 \times 10^{-11}$	(Burkholder et al., 2019)

$BrO + NO_2 (+M) \rightarrow BrONO_2 (+M)$	$k_0 = 5.5 \times 10^{-31} \times (T/298)^{-3.1}$ $k_\infty = 6.6 \times 10^{-11} \times (T/298)^{-2.9}$	(Burkholder et al., 2019)
$Br + NO_2 (+M) \rightarrow BrNO_2 (+M)$	$k_0 = 4.3 \times 10^{-31} \times (T/298)^{-2.4}$ $k_\infty = 2.7 \times 10^{-11}$	(Burkholder et al., 2019)
$IO + NO_2 (+M) \rightarrow IONO_2 (+M)$	$k_0 = 7.7 \times 10^{-31} \times (T/298)^{-3.5}$ $k_\infty = 7.7 \times 10^{-12} \times (T/298)^{-1.5}$	(Burkholder et al., 2019)
Thermal decomposition	s^{-1}	
$BrONO_2 \rightarrow BrO + NO_2$	$2.8 \times 10^{13} \times e^{(-12360/T)}$	(Orlando and Tyndall, 1996)
Photolysis rates of gas phase species	Reference for absorption cross section and quantum yield	
$BrO + h\nu \rightarrow Br + O$		(Atkinson et al., 2004)
$HOBr + h\nu \rightarrow Br + OH$		(Atkinson et al., 2004)
$BrONO_2 + h\nu \rightarrow BrO + NO_2$		(Atkinson et al., 2004)
$BrONO_2 + h\nu \rightarrow Br + NO_3$		(Atkinson et al., 2004)
$BrNO_2 + h\nu \rightarrow Br + NO_2$		(Atkinson et al., 2004)
$HOI + h\nu \rightarrow I + OH$		(Atkinson et al., 2004)
$IO + h\nu \rightarrow I + O$		(Atkinson et al., 2004)
$OIO + h\nu \rightarrow I + O_2$		(Atkinson et al., 2004)

4 References

Atkinson, R., Baulch, D. L., Cox, R. A., Crowley, J. N., Hampson, R. F., Hynes, R. G., Jenkin, M. E., Rossi, M. J., and Troe, J.: IUPAC Task Group on Atmospheric Chemical Kinetic Data Evaluation, Atmos. Chem. Phys., 4, 2004.

Atkinson, R., Baulch, D. L., Cox, R. A., Crowley, J. N., Hampson, R. F., Hynes, R. G., Jenkin, M. E., Rossi, M. J., Troe, J., and Subcommittee, I.: Evaluated kinetic and photochemical data for atmospheric chemistry: Volume II – gas phase reactions of organic species, Atmos. Chem. Phys., 6, 3625-4055, 10.5194/acp-6-3625-2006, 2006.

Atkinson, R., Baulch, D. L., Cox, R. A., Crowley, J. N., Hampson, R. F., Hynes, R. G., Jenkin, M. E., Rossi, M. J., and Troe, J.: Evaluated kinetic and photochemical data for atmospheric chemistry: Volume III – gas phase reactions of inorganic halogens, Atmos. Chem. Phys., 7, 981-1191, 10.5194/acp-7-981-2007, 2007.

Bohn, B., Heard, D. E., Mihalopoulos, N., Plass-Dülmer, C., Schmitt, R., and Whalley, L. K.: Characterisation and improvement of j(O1D) filter radiometers, Atmos. Meas. Tech., 9, 3455-3466, 10.5194/amt-9-3455-2016, 2016.

Bohn, B., and Lohse, I.: Calibration and evaluation of CCD spectroradiometers for ground-based and airborne measurements of spectral actinic flux densities, Atmos. Meas. Tech., 10, 3151-3174, 10.5194/amt-10-3151-2017, 2017.

Burkholder, J. B., Sander, S. P., Abbatt, J., Barker, J. R., Cappa, C., Crounse, J. D., Dibble, T. S., Huie, R. E., Kolb, C. E., Kurylo, M. J., Orkin, V. L., Percival, C. J., Wilmouth, D. M., and Wine, P. H.: Chemical Kinetics and Photochemical Data for Use in Atmospheric Studies, Evaluation No. 19, JPL Publication 19-5, Jet Propulsion Laboratory, Pasadena, 2019.

Gómez Martín, J. C., Spietz, P., and Burrows, J. P.: Kinetic and Mechanistic Studies of the I2/O3 Photochemistry, The Journal of Physical Chemistry A, 111, 306-320, 10.1021/jp061186c, 2007.

Orlando, J. J., and Tyndall, G. S.: Rate Coefficients for the Thermal Decomposition of BrONO2 and the Heat of Formation of BrONO2, The Journal of Physical Chemistry, 100, 19398-19405, 10.1021/jp9620274, 1996.

Riffault, V., Bedjanian, Y., and Poulet, G.: Kinetic and mechanistic study of the reactions of OH with IBr and HOI, Journal of Photochemistry and Photobiology A: Chemistry, 176, 155-161, https://doi.org/10.1016/j.jphotochem.2005.09.002, 2005.